Journal of Scientific Computing, Vol. 12, No. 2, 1997

Numerical Simulation of Low Mach Number Reactive Flows

A. G. Tomboulides,[1,2] J. C. Y. Lee,[1,2] and S. A. Orszag[1]

Received October 11, 1996

A new formulation for the numerical solution of low Mach number compressible flow problems is presented and analyzed. In this formulation the thermal part (energy and species equations) is solved implicitly and decoupled from the momentum equation, whereas the hydrodynamic part (momentum-continuity) is advanced in time using a high order splitting approach which results in overall high order accuracy in time and minimal errors in mass conservation. These errors are analyzed using both analytical tools and benchmark numerical examples. Results from two-dimensional simulations with one-step global reaction in opposed jet flame and porous particle configurations are also presented.

KEY WORDS: Combustion; numerical simulation; opposed jet flames; porous particle combustion; splitting method.

1. INTRODUCTION

In the numerical solution of low speed compressible reacting flows involved in combustion problems, the existence of high frequency acoustic waves places a severe restriction on time steps. One can use regular perturbation techniques to decouple acoustic waves from the equations (when they are not of interest). In this work, a set of approximate equations, free of acoustic wave interactions [Chu and Kovasznay (1958); Sivashinsky (1979); and Rehm and Baum (1978)] are obtained, where pressure appears at leading order in the energy and state equations ("thermodynamic

[1] Mechanical and Aerospace Engineering, Princeton University, Princeton, New Jersey 08544.
[2] Present address: ETH, Zurich Switzerland.

0885-7474/97/0600-0139$12.50/0

pressure" p_0), and at first order in the momentum equation ("hydrodynamic pressure" p_1). The resulting equations, when the Mach number approaches zero, are

$$\rho c_p \left(\frac{\partial T}{\partial t} + \mathbf{v} \cdot \nabla T \right) = \nabla \cdot \lambda \nabla T + \sum_{i=1}^{N} h_i^0 \dot{w}_i - \nabla \cdot \rho T \sum_{i=1}^{N} c_{p,i} Y_i \mathbf{V}_i + \frac{\partial p_0}{\partial t} \tag{1.1a}$$

$$\rho \left(\frac{\partial Y_i}{\partial t} + \mathbf{v} \cdot \nabla Y_i \right) = -\nabla \cdot \rho Y_i \mathbf{V}_i + \dot{w}_i, \qquad i = 1,\ldots, N \tag{1.1b}$$

$$p_0 = \rho R T \tag{1.1c}$$

$$\rho \left(\frac{\partial \mathbf{v}}{\partial t} + \mathbf{v} \cdot \nabla \mathbf{v} \right) = -\nabla p_1 + \nabla \cdot \mu \left(\underline{\underline{\nabla \mathbf{v}}} + (\underline{\underline{\nabla \mathbf{v}}})^T - \frac{2}{3} (\nabla \cdot \mathbf{v}) \underline{\underline{\mathbf{I}}} \right) \tag{1.1d}$$

$$\frac{\partial \rho}{\partial t} + \mathbf{v} \cdot \nabla \rho = \rho \nabla \cdot \mathbf{v} \tag{1.1e}$$

where $\mathbf{v}$ is the velocity field, T the temperature, and ρ the density. In addition Y_i, $\mathbf{V}_i$ are the mass fraction, and diffusion velocity—defined for example in Williams (1985)—of the ith species, whereas h_i^0 and $\dot{w}_i$ are the heat of formation and rate of production of the ith species respectively; μ, λ are the dynamic viscosity, and heat conductivity, respectively, whereas $c_{p,i}$ is the specific heat capacity of species i; D_{ij} which appears in the definition of $\mathbf{V}_i$ is the binary diffusion coefficient of species i and j.

All of these equations, except Eq. (1.1d), are derived from the balance of ε^0 (where $\varepsilon = \gamma M^2$, where γ is the ratio of specific heats and M is the Mach number) terms. The leading order momentum equation reduces to $\nabla p_0 = 0$; therefore, p_0 can only be a function of time. In an open system, where the pressure has to approach a constant value at infinity (i.e., atmospheric pressure) the last term in the energy equation (1.1a) vanishes. All quantities that appear in these equations, are the leading order terms (ε^0) of their corresponding ε expansion, except for the hydrodynamic pressure $p_1(\mathbf{x}, t)$, which appears on the right side of the momentum equation (1.1d) and is a first order (ε^1) quantity.

Several approaches have been used in the past for the integration of Eqs. (1.1a)–(1.1e). A chemically reactive flow system involves hydrodynamics, diffusive transport, and thermo-chemistry. Even the simplest one-dimensional flame models can typically be solved analytically only under additional simplifications such as steady-state, constant and equal diffusivities of all species, and infinitely fast chemistry. Numerical methods are generally required to obtain solutions if any realistic transport and chemical kinetics are included. Numerical models of steady premixed and

non-premixed flames [for example, see Kee *et al.*, (1985), and Lutz *et al.*, (1994)], have long been utilized to complement experiments. Results obtained with these one-dimensional models on strained flames are also used in flamelet modeling of turbulent flames. Recently, transient one-dimensional models have also been developed to simulate spherically symmetric combustion systems such as a droplet or fuel particle gasifying in a quiescent environment [Cho *et al.*, (1992); Lee *et al.*, (1995, 1996a)].

However, practical reactive flow systems are inherently two-or three-dimensional. In fact, some phenomena such as the instability of a lean hydrogen-air premixed flame can only be explained in a two-dimensional context. A large class of chemically reactive flow problems are axisymmetric and, thus, at least two-dimensional; examples include isolated fuel particle combustion systems (in which particles move relative to a quiescent environment), laminar flow reactors, concentric co-flowing non-premixed flames, and *air/fuel* mixtures ignited by individual hot particles. The important case of an opposed-jet configuration, which is used extensively to obtained experimental data on one-dimensional strained flames (premixed and non-premixed), is also a two-dimensional system.

Numerical modeling of two-dimensional chemically reactive compressible flows with detailed chemistry and transport is just beginning and, to date, have been mainly limited to steady-state simulations [for example, see Xu *et al.* (1993); Ern *et al.* (1994); and Smooke *et al.* (1989), where numerical simulations of a steady-state axisymmetric gas-jet non-premixed methane flame are reported]. A review of different methods used for the simulation of reactive flows can be found in Oran and Boris (1987). In Patnaik *et al.* (1988) and Behrent *et al.* (1992), the focus is on the investigation of instabilities of a one-dimensional premixed hydrogen/air flame in a rectangular box, whereas in Dwyer (1990) and Dwyer and Sanders (1988), transient simulations of octane droplet combustion in an oxidizer stream are reported. In the latter, although diffusive transport is treated in detail, the chemistry is described by a one-step global reaction. The effects of internal circulation and heat transfer on the time-dependent vaporization of a droplet in the absence of chemical reactions is reported in Patnaik *et al.* (1985) and Megaridis and Sirignano (1992). These two-dimensional numerical simulations are based on either finite difference or finite volume methods. Recently, two-and three-dimensional simulations of turbulent flows with simple and detailed chemistry have also been reported (a review of such simulations can be found in Poinsot *et al.* (1996)). In this work, the low Mach number approximation is not employed and the nonreduced equations are solved using a high-order finite difference scheme.

Here, we present and analyze a new numerical approach for the integration of the governing equations (1.1a)–(1.1e). In order to facilitate

the presentation (but not the implementation of the method in actual computations), several simplifying assumptions will be made. First, detailed transport processes are neglected, and only singlestep (global) reaction mechanisms are considered. This means that all species have the same molecular weight, specific heat capacity, and binary diffusion coefficient. In addition, all dynamic transport coefficients μ, λ, ρD, and specific heat capacity c_p are assumed to be independent of temperature, so that the kinematic transport coefficients ν, α, and D become directly proportional to temperature. In addition, thermodynamic pressure is assumed to be constant in time as well as in space, corresponding to open systems. These assumptions, however, are not necessary and are only made to simplify the presentation of the numerical scheme. Detailed transport modeling and comprehensive chemical reaction mechanisms have also been implemented and are reported in Lee *et al.* (1996b, 1997); Lee (1996).

After nondimensionalization with appropriate reference quantities, and incorporation of all the simplifying assumptions, the following system is obtained:

$$\frac{\partial \tilde{T}}{\partial \tilde{t}} + \tilde{\mathbf{v}} \cdot \tilde{\nabla} \tilde{T} = \frac{\tilde{\alpha}}{Re\, Pr} \tilde{\nabla}^2 \tilde{T} + Da \sum_{i=1}^{N} \tilde{h}_i^0 \dot{\tilde{w}}_i' \tag{1.2a}$$

$$\frac{\partial \tilde{Y}_i}{\partial \tilde{t}} + \tilde{\mathbf{v}} \cdot \tilde{\nabla} \tilde{Y}_i = \frac{\tilde{D}}{Re\, Sc} \tilde{\nabla}^2 Y_i + Da\, \dot{\tilde{w}}_i', \qquad i = 1, \ldots, N \tag{1.2b}$$

$$1 = \tilde{\rho} \tilde{T} \tag{1.2c}$$

$$\frac{\partial \tilde{\mathbf{v}}}{\partial \tilde{t}} + \tilde{\mathbf{v}} \cdot \tilde{\nabla} \tilde{\mathbf{v}} = -\frac{1}{\tilde{\rho}} \tilde{\nabla} \tilde{p}_1 + \frac{\tilde{\nu}}{Re} \left(\tilde{\nabla}^2 \tilde{\mathbf{v}} + \frac{1}{3} \tilde{\nabla} (\tilde{\nabla} \cdot \tilde{\mathbf{v}}) \right) \tag{1.2d}$$

$$\tilde{\nabla} \cdot \tilde{\mathbf{v}} = \frac{1}{Re\, Pr} \tilde{\nabla}^2 \tilde{T} + Da \sum_{i=1}^{N} \frac{\tilde{h}_i^0}{\tilde{T}} \dot{\tilde{w}}_i' \tag{1.2e}$$

All variables with tildes are nondimensional, whereas Re, Pr, and Sc are the Reynolds, Prandtl, and Schmidt numbers respectively, Da is the pre-exponential Damköhler number of the one-step reaction, and $\tilde{\alpha} = \tilde{D} = \tilde{\nu} = \tilde{T}$. The continuity equation (1.1e) is replaced by Eq. (1.2e), which has been obtained from Eqs. (1.1e), (1.1a), and (1.1c). It can be observed from Eq. (1.2e) that the only sources for nonzero divergence of the velocity field are the heat released by chemical reactions and diffusive heat transfer (and, for closed systems only, global compression or expansion). The reaction rate term $\dot{\tilde{w}}_i'$ is described by a one-step global reaction, with the reaction rate written in the Arrhenius form.

2. NUMERICAL APPROACH

In this section, the solution of the semi-discrete problem is discussed (where only temporal but not spatial derivatives are discretized). The overall system can be considered as a differential algebraic system of the form,

$$\frac{\partial \mathbf{y}}{\partial t} = \mathbf{f}(\mathbf{y}(\mathbf{x}, t)) \tag{2.1a}$$

$$0 = g(\mathbf{y}(\mathbf{x}, t)) \tag{2.1b}$$

where $\mathbf{y} = \{T, Y_i, \mathbf{v}\}^T$. The predictive equations for $\mathbf{y}$, Eq. (2.1a), correspond to Eqs. (1.2a)–(1.2b), and (1.2d), whereas the algebraic Eq. (2.1b) corresponds to Eq. (1.2e). The state Eq. (1.2c) has been used to eliminate density from the rest of the equations. Equation (2.1b) can be seen as a constraint on the velocity field which is necessary in order to close the system for the extra unknown p_1, for which there is no predictive equation. In a fully implicit solution of this nonlinear system based on high order backward differentiation (or stiffly stable schemes, Gear (1971)) all variables have to be evaluated at the new time level t^{n+1}. The fully implicit approach, however, is quite expensive and a combined implicit/explicit approach, which preserves high order accuracy in time, is preferable.

All the terms in the energy (1.2a) and species (1.2b) equations are advanced in time implicitly, because of the presence of chemical reaction source terms (which in general involves different time scales and introduces stiffness), except for the convective terms for which a high-order explicit extrapolation for the velocity is used. On the other hand, since there is no direct reaction source term in the momentum equations, the velocity field responds to changes in temperature and density on a slower inertial time scale. Therefore the integration of Eq. (1.2d), can be performed with a semi-implicit splitting method, where the updated temperature and species fields are used to determine density, from Eq. (1.2c), divergence of the velocity field from Eq. (1.2e) and kinematic viscosity. The integration then proceeds in the following way (dropping tildes for clarity)

$$\frac{1}{\Delta t}\sum_{q=0}^{J} \alpha_q T^{n+1-q} = -\left(\sum_{q=0}^{J-1} \beta_q \mathbf{v}^{n-q}\right)\cdot \nabla T^{n+1} + \frac{\alpha}{Re\, Pr}\nabla^2 T^{n+1} + Da \sum_{i=1}^{N} h_i^0 \dot{w}_i' \tag{2.2a}$$

$$\frac{1}{\Delta t}\sum_{q=0}^{J} \alpha_q Y_i^{n+1-q} = -\left(\sum_{q=0}^{J-1} \beta_q \mathbf{v}^{n-q}\right)\cdot \nabla Y_i^{n+1} + \frac{D}{Re\, Sc}\nabla^2 Y_i^{n+1} + Da\, \dot{w}_i' \tag{2.2b}$$

$$Q_T^{n+1} = \frac{1}{Re\,Pr}\nabla^2 T^{n+1} + Da \sum_{i=1}^{N} \frac{h_i^0 \dot{w}_i'}{T^{n+1}} \tag{2.2c}$$

$$\frac{1}{\Delta t}\sum_{q=0}^{J} \alpha_q \mathbf{v}^{n+1-q} = -\sum_{q=0}^{J-1} \beta_q (\mathbf{v}\cdot\nabla\mathbf{v})^{n-q} - \frac{1}{\rho}\nabla p_1 + \frac{\nu}{Re}\left(\nabla^2\mathbf{v} + \frac{1}{3}\nabla(\nabla\cdot\mathbf{v})\right)^{n+1} \tag{2.2d}$$

Here, Q_T^{n+1} is the "thermal" divergence of the velocity field, and α_q, β_q are the coefficients of the implicit and explicit, respectively, part of the Jth order time integration scheme [Orszag *et al.* (1986); Karniadakis *et al.* (1991); Tomboulides *et al.* (1989)]. All quantities which are functions of temperature and species mass fractions in the general case, (α, D, ν, ρ, and $\dot{w}_i'$) are evaluated using T^{n+1} and Y_i^{n+1}. The convective terms in all equations are integrated explicitly or semi-explicitly. Since the velocity field used in Eqs. (2.2a) and (2.2b) is known, these equations can be solved independently as a system of $N+1$ equations for T^{n+1}, and Y_i^{n+1}. A sparse-Jacobian stiff ODE solver (LSODES, Hindmarsh (1983)), is used for this integration because in general the behavior of these equations will be affected by the stiffness of the chemical reaction mechanism. The integration order in principle can be up to fifth.

After determining all thermodynamic quantities (temperature T^{n+1}, and species concentrations Y_i^{n+1}) at the new time level t^{n+1}, all kinematic transport coefficients α, D, ν and density ρ, which are functions of T^{n+1}, are also known. The integration of Eqs. (2.2c), and (2.2d) is performed using a mixed explicit-implicit splitting approach which results in an overall high order of accuracy in time, minimal errors in mass conservation, and a partially decoupled solution procedure. The time integration method is based on backward differentiation and is the same scheme used for the integration of the energy and species equations. In addition, a pressure Poisson equation, similar to that for incompressible flows, is derived for the hydrodynamic pressure p_1, accounting for the nonzero thermal divergence of the velocity field, which can be considered as a constraint enforced by the hydrodynamic pressure.

The integration of the momentum equation (2.2d) is explicit for the nonlinear convective terms, and implicit for the viscous and pressure terms. It proceeds in the following way, starting with the integration of the convective terms

$$\frac{\mathbf{v}^*}{\Delta t} - \frac{1}{\Delta t}\sum_{q=0}^{J-1} \alpha_q \mathbf{v}^{n-q} = -\sum_{q=0}^{J-1} \beta_q (\mathbf{v}\cdot\nabla\mathbf{v})^{n-q} \tag{2.3}$$

which can be solved to obtain $\mathbf{v}^*$. Then a variable coefficient Poisson equation is derived for the pressure p_1, by taking the divergence of equation (2.2d), to obtain

$$\nabla\cdot\left(\frac{\nabla p_1}{\rho^{n+1}}\right)=\frac{\nabla\cdot\mathbf{v}^*-\gamma_0(\nabla\cdot\mathbf{v})^{n+1}}{\Delta t}+\frac{1}{Re}\nabla\cdot\nu^{n+1}\left(\nabla^2\mathbf{v}+\frac{1}{3}\nabla(\nabla\cdot\mathbf{v})\right)^{n+1} \tag{2.4}$$

In order to decouple the pressure and velocity calculation, the terms involving ν^{n+1} in the pressure equation have to be expressed in terms of known quantities. This is performed using the identity

$$\nabla^2\mathbf{v}=\nabla(\nabla\cdot\mathbf{v})-\nabla\times(\nabla\times\mathbf{v})$$

which results in

$$\nabla\cdot\left(\frac{\nabla p_1}{\rho^{n+1}}\right)=\frac{\nabla\cdot\mathbf{v}^*-\gamma_0(\nabla\cdot\mathbf{v})^{n+1}}{\Delta t}+\frac{1}{Re}\nabla\cdot\nu^{n+1}\left(\frac{4}{3}\nabla(\nabla\cdot\mathbf{v})-\nabla\times(\nabla\times\mathbf{v})\right)^{n+1} \tag{2.5}$$

Using an irrational-solenoidal decomposition of the velocity field $\mathbf{v}=\mathbf{v}_S+\mathbf{v}_I$, and treating terms involving $\mathbf{v}_I$ implicitly (using the known "thermal" divergence of the velocity field, Q_T^{n+1}) as

$$(\nabla\cdot\mathbf{v})^{n+1}=(\nabla\cdot\mathbf{v}_I)^{n+1}\approx Q_T^{n+1}$$

while an explicit extrapolation for the solenoidal part, results in

$$(\nabla\times\mathbf{v})^{n+1}=(\nabla\times\mathbf{v}_S)^{n+1}\approx\sum_{q=0}^{j-1}\beta_q\boldsymbol{\omega}^{n-q}$$

where $\boldsymbol{\omega}=\nabla\times\mathbf{v}$ is the vorticity. This procedure is similar to splitting methods used for incompressible flows, discussed in detail by Orszag *et al.* (1986). Substituting the last two expressions in Eq. (2.5), results in the following pressure Poisson equation

$$\nabla\cdot\left(\frac{\nabla p_1}{\rho^{n+1}}\right)=\frac{\nabla\cdot\mathbf{v}^*-\gamma_0 Q_T^{n+1}}{\Delta t}+\frac{1}{Re}\nabla\cdot\nu^{n+1}\left(\frac{4}{3}\nabla Q_T^{n+1}-\sum_{q=0}^{J-1}\beta_q\nabla\times\boldsymbol{\omega}^{n-q}\right) \tag{2.6}$$

which now does not involve the unknown velocity $\mathbf{v}^{n+1}$. The boundary conditions for the pressure equation are derived by taking the dot product of Eq. (2.2d) in the direction normal to the boundaries $\mathbf{n}$, and making the substitutions mentioned earlier. In this way, a Neumann pressure boundary condition is obtained when the velocity satisfies Dirichlet boundary conditions, namely,

$$\frac{1}{\rho^{n+1}}\frac{\partial p_1}{\partial n} = -\frac{\partial(\mathbf{n}\cdot\mathbf{v})}{\partial t} - \mathbf{n}\cdot\sum_{q=0}^{J-1}\beta_q(\mathbf{v}\cdot\nabla\mathbf{v})^{n-q} + \frac{\nu^{n+1}}{Re}\mathbf{n}\cdot\left(\frac{4}{3}\nabla Q_T^{n+1} - \sum_{q=0}^{J-1}\beta_q\nabla\times\boldsymbol{\omega}^{n-q}\right) \tag{2.7}$$

where the first term in the righthand side of Eq. (2.7) is assumed to be known for Dirichlet velocity boundary conditions. The rest of the splitting scheme consists of the incorporation of the pressure correction to the velocity field, and then integration of the viscous part of the momentum equation in the following two steps

$$\frac{\mathbf{v}^{**}-\mathbf{v}^{*}}{\Delta t} = -\frac{\nabla p_1}{\rho^{n+1}} \tag{2.8}$$

$$-\frac{\nu^{n+1}}{Re}\nabla^2\mathbf{v}^{n+1} + \frac{\gamma_0\mathbf{v}^{n+1}}{\Delta t} = \frac{\mathbf{v}^{**}}{\Delta t} + \frac{1}{3}\frac{\nu^{n+1}}{Re}\nabla Q_T^{n+1} \tag{2.9}$$

The boundary conditions for the velocity are incorporated in the viscous step as well. The solution procedure is then completed by choosing a method for the spatial discretization. The methods used in this work are either global spectral methods or spectral element methods, which are extensively described in Gottlieb and Orszag (1977); Canuto *et al.* (1987); Patera (1984); Rønquist (1988); Karniadakis *et al.* (1985); and Maday and Patera (1987).

In the following sections, it will be demonstrated that the splitting procedure described in this section gives an overall high order of accuracy in time, and minimal errors in mass conservation (the so-called splitting errors). The behavior of these errors is obtained using asymptotic analysis; it is shown that splitting errors are always smaller than the formal truncation error $\mathcal{O}(\Delta t^J)$ of the Jth order integration scheme. In addition, the asymptotically derived estimates are compared with results obtained from the numerical solution of a quasi two-dimensional model problem. The detailed description of the two-dimensional model problem, which is used for this comparison is presented in Tomboulides and Orszag (1997).

3. ERROR IN MASS CONVERSATION DUE TO SPLITTING

In order to obtain an estimate for the splitting errors, an equation for the difference between the divergence of the velocity field $Q^{n+1} = \nabla \cdot \mathbf{v}^{n+1}$ and the "thermal" divergence Q_T^{n+1} [see (2.2c)] is obtained. The thermal divergence Q_T^{n+1} can be considered as a constraint on the velocity field, in the same way that the condition $\nabla \cdot \mathbf{v} = 0$ is a constraint for incompressible flow. The equation for the difference $\phi = Q^{n+1} - Q_T^{n+1}$, can be obtained by subtracting the divergence of Eq. (2.9), after using Eq. (2.8), from Eq. (2.2d):

$$\frac{\gamma_0 Q^{n+1} - \nabla \cdot \mathbf{v}^*}{\Delta t} + \nabla \cdot \left(\frac{\nabla p_1}{\rho^{n+1}} \right) = \nabla \cdot \frac{\nu^{n+1}}{Re} \left(\nabla^2 \mathbf{v}^{n+1} + \frac{1}{3} \nabla Q_T^{n+1} \right) \tag{3.1}$$

which, using Eq. (2.6), yields

$$\frac{\gamma_0}{\Delta t} \phi - \nabla \cdot \frac{\nu^{n+1}}{Re} \nabla \phi = -\nabla \cdot \frac{\nu^{n+1}}{Re} \left(\nabla \times \boldsymbol{\omega}^{n+1} - \sum_{q=0}^{J-1} \beta_q \nabla \times \boldsymbol{\omega}^{n-q} \right) \tag{3.2}$$

This is an elliptic (variable coefficient Helmholtz) equation for the difference $\phi = Q^{n+1} - Q_T^{n+1}$, between the divergence at time step t^{n+1} and the value dictated by the energy equation from Eq. (2.2c). The right-hand side of this elliptic equation is nonzero only when the viscosity is variable, since, for ν constant in space, it is identically equal to zero because of the vector identity $\nabla \cdot (\nabla \times \boldsymbol{\omega}) = 0$. In addition, this term is of order $\mathcal{O}(\Delta t^J)$, where J is the order of the time stepping scheme used (typically up to $J = 3$); its maximum value is $\mathcal{O}(\Delta t)$ which corresponds to a first order scheme. To find the boundary condition for (3.2), the boundary condition for the divergence Q^{n+1},

$$\frac{1}{\rho^{n+1}} \frac{\partial p_1}{\partial n} = -\mathbf{n} \cdot \sum_{q=0}^{J-1} \beta_q (\mathbf{v} \cdot \nabla \mathbf{v})^{n-q} + \frac{\nu^{n+1}}{Re} \mathbf{n} \cdot \left(\frac{4}{3} \nabla Q^{n+1} - \nabla \times \boldsymbol{\omega}^{n+1} \right) \tag{3.3}$$

should be subtracted from the numerical pressure boundary condition (2.8), to obtain the following Neumann boundary condition

$$\frac{4}{3} \frac{\partial \phi}{\partial n} = \mathbf{n} \cdot \left(\nabla \times \boldsymbol{\omega}^{n+1} - \sum_{q=0}^{J-1} \beta_q \nabla \times \boldsymbol{\omega}^{n-q} \right) \tag{3.4}$$

Both Eq. (3.2) satisfied by ϕ and its boundary condition (3.4) have a nonhomogeneous part which scales with $\mathcal{O}(\Delta t^J)$. The nonzero boundary condition (3.4) is the cause of splitting errors that also appear in incompressible flows [i.e., the homogeneous solution of (3.2)], whereas the

nonzero right-hand side of Eq. (3.2) is the part of the error which is caused by the compressibility, only when the kinematic viscosity is spatially varying [i.e., the particular solution of (3.2)].

In this section, the error in mass conservation due to splitting will be analyzed for the case of small values of $\Delta t/Re$. A one-dimensional problem, which incorporates most of the important features of the problem, is used for asymptotic analysis. It is assumed that the temperature T varies in layers of thickness much larger than the length scale $(\Delta t/Re)^{1/2}$. This means that if the temperature has a local structure similar to $\tanh(x/\delta)$, typical of flame fronts, then the length scale $\delta \gg (\Delta t/Re)^{1/2}$. The domain of interest extends from $x=-1$ to $x=+1$, and the boundary conditions are derived from (3.4). Equation (3.2) in one dimension, becomes

$$\varepsilon^2\phi'' + \varepsilon^2 a(x)\,\phi' + b(x)\,\phi = \varepsilon^2 a(x)\,\Delta\omega_s \tag{3.5}$$

with the boundary conditions

$$\phi'(\pm 1) = \tfrac{3}{4}\,\Delta\omega_s\,|_{\pm 1} \tag{3.6}$$

Here, $\phi = Q^{n+1} - Q_T^{n+1}$, $\Delta\omega_s = \nabla\times\boldsymbol{\omega}^{n+1} - \sum_{q=0}^{J-1}\beta_q \nabla\times\boldsymbol{\omega}^{n-q}$, and $\varepsilon = (\Delta t/Re)^{1/2}$. The functions $a(x)$ and $b(x)$ are given by $a(x) = T'/T$, and $b(x) = -1/T$. It will be assumed later that, for a Jth order time stepping method, $\Delta\omega_s$ if of $\mathcal{O}(\Delta t^J)$ everywhere, in order to get global estimates for ϕ. Equation (3.5) is a nonhomogeneous singularly perturbed ordinary differential equation. The problem is divided into two separate problems, one with nonzero right-hand side and zero boundary conditions (a particular solution ϕ_P, corresponding to errors due to compressibility), and one with zero right-hand side and nonzero boundary conditions (a homogeneous solution ϕ_H, corresponding to classical incompressible splitting errors). A particular solution to Eq. (3.5) is found by first constructing the Green's function of the differential operator using the WKB method [Bender and Orszag (1978)], and then finding the particular solution of the nonhomogeneous problem. Applying WKB, it is found that the general solution of (3.5) has to $\mathcal{O}(\varepsilon)$ the following form

$$\phi(x) = A_{\pm}\,T^{-1/4}\exp\left(\pm\frac{1}{\varepsilon}\int^{x}\frac{dt}{T^{1/2}(t)}\right) \tag{3.7}$$

where $A_{\pm}$ are constants to be specified by the boundary conditions. The solutions ϕ_P and ϕ_H are found, to leading order, to be

$$\phi_P(x) = \varepsilon^2\,\Delta\omega_s T'(x) + \mathcal{O}(\varepsilon^4\Delta\omega_s) \tag{3.8}$$

$$\phi_H(x) = \tfrac{3}{4}\varepsilon\,\Delta\omega_s\,|_{\pm 1}\,T^{-1/4}(x)\,f(x) + \mathcal{O}(\varepsilon^2\,\Delta\omega_s\,|_{\pm 1}) \tag{3.9}$$

This means that if the quantity $\Delta\omega_s$ is globally of order Δt or $\varepsilon^2 Re$ (for a first order overall scheme), the overall error in the interior of the domain, due to the inhomogeneity on the right-hand side of (3.5), is of $\mathcal{O}(\Delta t^2/Re)$. Similarly, the error in the interior for a time integrating scheme of order J would by $\mathcal{O}(\Delta t^{J+1}/Re)$. For simplicity we have assumed that $\Delta\omega_s(-1) = \Delta\omega_s(+1) = \Delta\omega_s(\pm 1)$. On the other hand, assuming again that $\Delta\omega_s(\pm 1)$ is $\mathcal{O}(\varepsilon^2 Re)$, the error close to the domain boundaries, which is due to the effect of nonhomogeneous boundary conditions, becomes $\mathcal{O}(\Delta t^{3/2}/Re^{1/2})$. This estimate is true in boundary layers of $\mathcal{O}(\varepsilon)$ close to the boundaries $x \sim \pm(1-\varepsilon)$, where the function $f(x)$ has an overall contribution of $\mathcal{O}(1)$. In the rest of the domain, the function $f(x)$ in Eq. (3.9) is exponentially small. Therefore, the error in mass conservation is of $\mathcal{O}(\Delta t^{J+1/2}/Re^{1/2})$ in a boundary layer of $\mathcal{O}(\varepsilon)$ away from the boundaries, and of $\mathcal{O}(\Delta t^{J+1}/Re)$ in the interior of the domain for a general Jth order time integration scheme.

In Fig. 1, we plot the distribution of the two sources of divergence error, the nonzero right side of (3.5) and the nonzero boundary condition (3.6), respectively. The plotted case is for $\varepsilon = 0.05$, $\delta = 0.1$, $Re = 1$ and $\Delta\omega_s = \varepsilon^2$, and corresponds to the temperature profile, also plotted in the same figure, $T = 0.5(3 + \tanh(x/\delta))$.

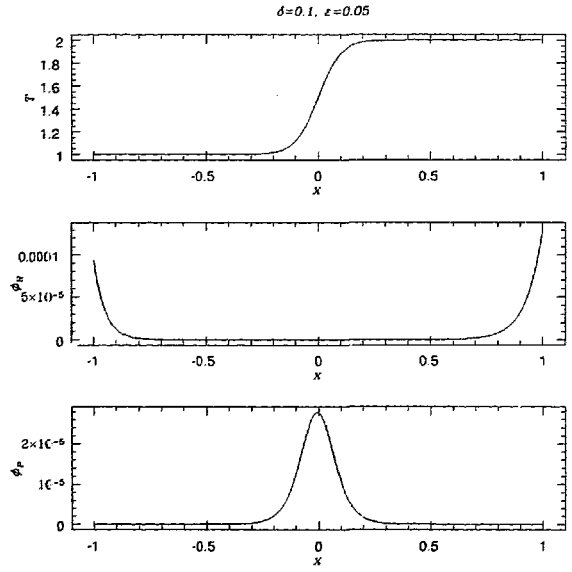

Fig. 1. Distribution of temperature, and divergence error for $\varepsilon = 0.05$, $\delta = 0.1$, and $\Delta\omega_s = \varepsilon^2$.

4. EXAMPLES OF REACTING FLOW SIMULATIONS

In this section, three examples of compressible reacting flows simulated using the numerical approach are presented. These examples include a quasi two-dimensional model problem formulated as a benchmark problem, an opposed jet non-premixed flame, and the gaseous burning of a porous sphere. All these examples involve simple transport and single-step reaction. Examples involving detailed transport and comprehensive chemistry are reported in [Lee *et al.* (1996b, 1997); Lee (1996)].

4.1. Model Problem

Having obtained an estimate for the structure and magnitude of splitting errors, a model problem is used here to verify the results of the asymptotic analysis and test all important aspects of the numerical solution procedure. For example, a simple one dimensional analytical solution would not be sufficient for this purpose, since in one dimension the right-hand side of the error equation (3.2) is identically zero, even for a variable kinematic viscosity. This is demonstrated by the numerical solution of the following one-dimensional example in the domain $-1 \leqslant x \leqslant 1$

$$\frac{\partial T_0}{\partial t} + U_0 \frac{\partial T_0}{\partial x} = \frac{\alpha}{Re\, Pr} \frac{\partial^2 T_0}{\partial x^2} + \dot{w}'_0 \tag{4.1a}$$

$$\frac{\partial U_0}{\partial t} + U_0 \frac{\partial U_0}{\partial x} = \frac{4\nu}{3\, Re} \frac{\partial^2 U_0}{\partial x^2} - \frac{1}{\rho_0} \frac{\partial P_1}{\partial x} \tag{4.1b}$$

$$\frac{\partial \rho_0}{\partial t} + U_0 \frac{\partial \rho_0}{\partial x} = -\rho_0 \frac{\partial U_0}{\partial x} \tag{4.1c}$$

$$\rho_0 T_0 = 1 \tag{4.1d}$$

In these non-dimensionalized equations $\nu = \alpha = T$. The reaction term in the energy equation is specified as

$$\dot{w}'_0 = \frac{1}{2\delta} \operatorname{sech}^2\left(\frac{x}{\delta}\right) + \frac{1}{\delta^2\, Re\, Pr} \tanh\left(\frac{x}{\delta}\right) \operatorname{sech}^2\left(\frac{x}{\delta}\right) \tag{4.2}$$

where the parameter δ corresponds to the thickness of the temperature layer, as in Fig. 1. The problem is closed by specifying the boundary conditions

$$U_0(\pm 1) = T_0(\pm 1) = \frac{1}{2}\left(3 + \tanh\left(\frac{\pm 1}{\delta}\right)\right)$$

The steady state solution of this problem is simply

$$U_0(x) = T_0(x) = \frac{1}{2}\left(3 + \tanh\left(\frac{x}{\delta}\right)\right) \tag{4.3}$$

and resembles a premixed flame located at $x = 0$ with reactants approaching the flame from the side $x = -1$, and products exiting the domain at $x = +1$. The reaction term (4.2) is chosen artificially to yield the flame front (4.3). The reaction term (4.2) does share some qualitative structure with that expected for premixed flames, but, due to the second term on the right side of (4.2), it has an artificial energy sink for $x < 0$ with $x \sim \delta$ and $Re\, Pr \leqslant O(1)$.

The numerical solution of this one-dimensional problem is obtained using the numerical approach described in Section 2. For the spatial discretization 4 spectral elements are used in the x direction, and the number of collocation points inside each of these elements varies from 5 to 15. It can be seen from the results plotted in Fig. 2 that the L_2 error of both the solution and of the divergence of the velocity field (as defined in Section 3), decay exponentially with the number of collocation points. This kind of exponential convergence is typical of spectral type methods; for this problem the magnitude of the error is not affected by the time step Δt, but only by the spatial discretization error, i.e., the errors in Fig. 2 are almost independent of the value of Δt. The reason for this is that the right-hand

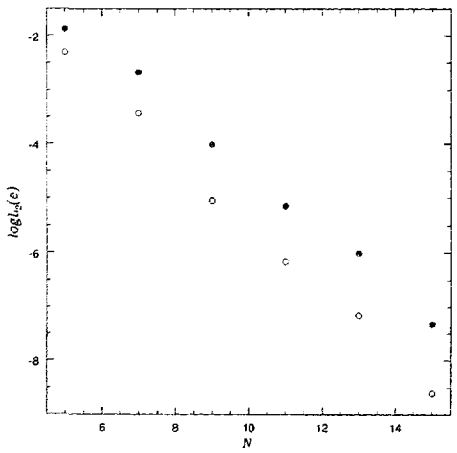

Fig. 2. Error $U_0 - U_{0c}$ and divergence error $\phi = \partial U_0/\partial x - Q_T$ as a function of number of collocation points for base flow of model problem.

side of Eq. (3.2) is identically equal to zero in one-dimension. In addition, the vorticity is identically equal to zero as well, and the boundary condition for the error in the divergence of the velocity field becomes homogeneous, as can be observed from Eq. (3.4). This implies that splitting errors are identically equal to zero in the whole domain, and the only source of error in obtaining the steady solution of system (4.1a)–(4.1d) is the spatial discretization error. Therefore, in order to test all aspects of our numerical method, a more complex model problem should be constructed.

Following the analysis in Orszag *et al.* (1986), a two-dimensional linear stability analysis was performed for the one-dimensional problem described by Eq. (4.3). The objective of this analysis is to obtain the least stable eigenmode. Subsequently, this least stable eigenmode was used as an initial condition for the time integration scheme described in Section 2 and the value of the decay rate (eigenvalue) and splitting errors were monitored during the integration. This new problem involving the integration of the two-dimensional linearized equations, has the features required to test the numerical scheme. A detailed account of the solution of this model problem is given in Tomboulides and Orszag (1997) and only some representative results are presented here.

In Fig. 3, the error in the value of the decay rate, as obtained by a time-dependent simulation of the linearized two-dimensional problem,

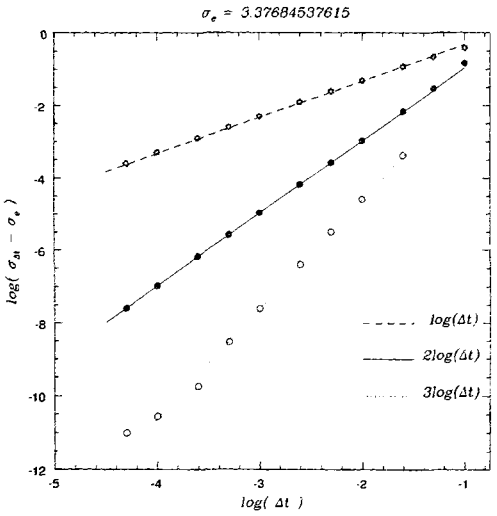

Fig. 3. Error in decay rate σ_r for $k = 1$ using different order integrating schemes.

using a 1^{st}, 2^{nd}, and 3^{rd} order time integration scheme, is shown. As can be observed from the figure, first, second and third order accuracy is obtained, respectively, for each of the schemes used, demonstrating the fact that splitting errors do not destroy the formal order of accuracy because they are of higher order.

The value of the error in mass conservation is plotted as a function of Δt in Fig. 4. The divergence error at the domain boundary (Fig. 4a) and at the middle of the domain (Fig. 4b) are plotted with points for different time stepping orders and values of Δt; also shown with lines are the asymptotic estimates obtained in Section 3. As can be observed, when the value of $\varepsilon=(\Delta t/Re)^{1/2}$ is small enough with respect to the "flame thickness" (here $\delta=0.2$), i.e., when $\Delta t \leqslant 0.01$ (for $Re=Pr=1$), the results of the asymptotic analysis agree well with the simulations. Also, for very low values of Δt, the errors for the third order in time scheme are very close to spatial discretization errors [with 257 Legendre points, with spatial error of $\mathcal{O}(10^{-12})$], and even to round-off error $\mathcal{O}(10^{-14})$, and the overall error saturates. Therefore, we conclude that the estimates obtained for the behavior of splitting errors are reliable and the overall accuracy of the numerical scheme is high.

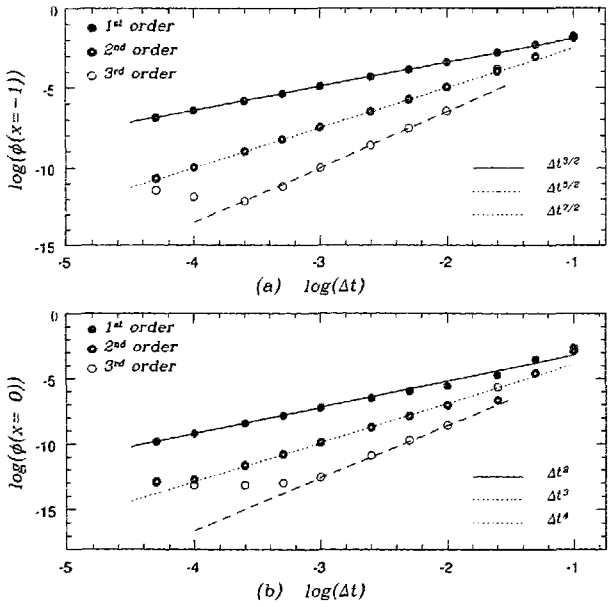

Fig. 4. Distribution of mass conservation errors at (a) $x=-1$; (b) $x=0$ respectively, for 1^{st}, 2^{nd}, and 3^{rd} order respectively.

4.2. Opposed Jet Flame

The transient two-dimensional numerical approach described here has been used in the simulation of an opposed-jet non-premixed flame, which is an important experimental configuration typically used to approximate a one-dimensional non-premixed flame [Law (1988)]. This experimental configuration offers the advantages of minimal heat losses, and nearly one-dimensional flame geometry in the vicinity of the stagnation plane (close to the axis of symmetry). In the limit of zero strain, quantitative information regarding one-dimensional non-premixed flames can be obtained by extrapolation. Traditionally, the non-premixed flame generated by this experimental configuration is analyzed in a one-dimensional context (see, for example [Law (1988)]), whereas, in theoretical studies, the flow field near the stagnation plane is described by a simple potential stagnation flow solution.

The assumption of potential stagnation flow, however, breaks down in areas far away from the stagnation plane, and one-dimensional analysis neglects cross streamline diffusion. The geometry of this experimental set-up in reality is at least two-dimensional (typically axially symmetric). Our numerical model can provide a full two-dimensional analysis of this experimental configuration, taking into account compressibility effects due to heat release in the flame zone.

Here we report axisymmetric simulations of a non-premixed counter flow configuration with one step chemistry and simple transport. The geometric setup and boundary conditions are shown in Fig. 5; the flow consists of two counter-flowing axial jets of fuel and oxidizer respectively. Also shown are two spectral element meshes (showing elements only): one consisting of 64 elements, and the other of 80 elements, which we used to adequately resolve the flame zone. The number of collocation points inside each element was varied between 7 and 9, in each direction. The reactant gases enter the domain with a nondimensional temperature of $T=1$, whereas the velocity profile at the exit of the tubes is parabolic; the Reynolds number is the same for both gases and is equal to $Re=UD/\nu=100$, where U is the mean exit velocity, D the diameter of the tube exit and ν the kinematic viscosity of the gases at the inlet temperature. The domain is constrained by two plates, located at the exit of the tubes, which are kept at a fixed temperature $T=1$, and it extends between $-0.5\leqslant z\leqslant 0.5$ and $0\leqslant r\leqslant 4$ (where all lengths are nondimensionalized by the tube diameter D). The chemistry is described by the one-step global reaction

$$\tfrac{1}{2}F+\tfrac{1}{2}O\rightarrow P \tag{4.4}$$

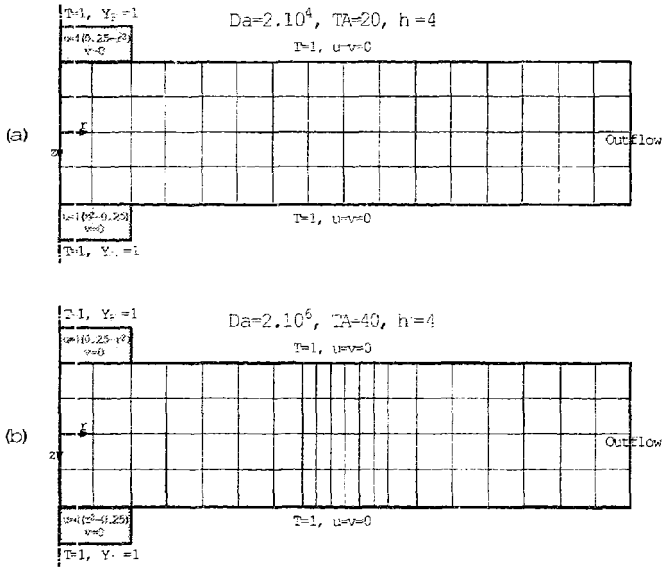

Fig. 5. Computational domain and spectral element mesh arrangement for (a) case I; (b) case II of the opposed jet configuration.

where F, O and P, are the fuel, oxidizer, and product, respectively, and the physical properties of all species are assumed to be equal. The reaction rate, appearing in Eq. (1.2a), is given by the following expression

$$\dot{w}' = Y_F^{1.2} Y_O^{1.2} e^{-T_A/T} \tag{4.5}$$

where no dependence on temperature has been assumed for the pre-exponential Arrhenius rate constant, and $T_A = E_A/R$ is the activation temperature. Two different numerical experiments were performed for this problem; in both, all parameters were kept fixed, except for the reaction rate parameters Da, T_A which were varied from $Da = 2 \times 10^4$ and $T_A = 20$ for case I, to $Da = 2 \times 10^6$ and $T_A = 40$ for case II (Da is the pre-exponential Damköhler number defined in Section 1). In case II, the reaction rate constants are such that the chemical induction time is longer, but the reaction time is shorter than case I.

In both cases, the ignition was performed by first obtaining the steady state solution for the cold flow and then igniting the flow using a high temperature strip close to the stagnation plane as an initial condition. Both simulations reached a steady state solution when integrated for long time; these steady state solutions are plotted in Figs. 6 and 7, for cases I and II,

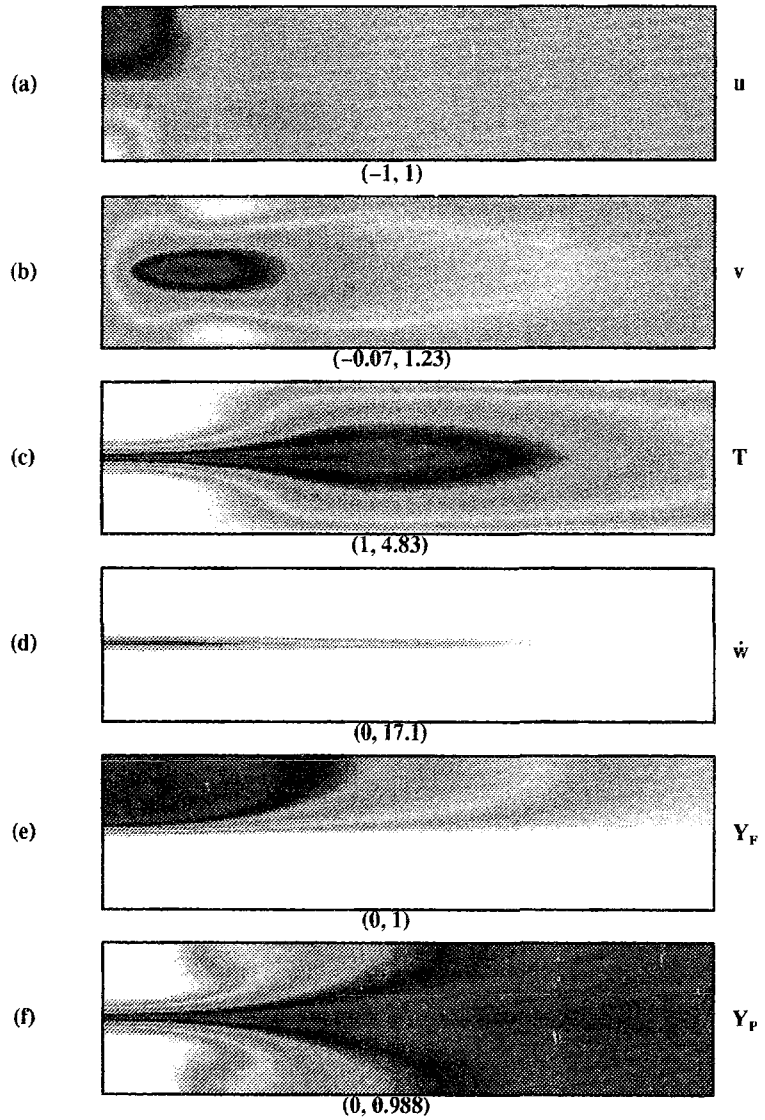

Fig. 6. Case I isocontours of (a) axial velocity; (b) radial velocity; (c) temperature; (d) reaction; (e) fuel mass fraction; and (f) product mass fraction. The minimum and maximum values of all variables are noted under each plot. Because this figure was generated by transformation of color plots to grey scale, the darkest tone does not correspond to the highest value.

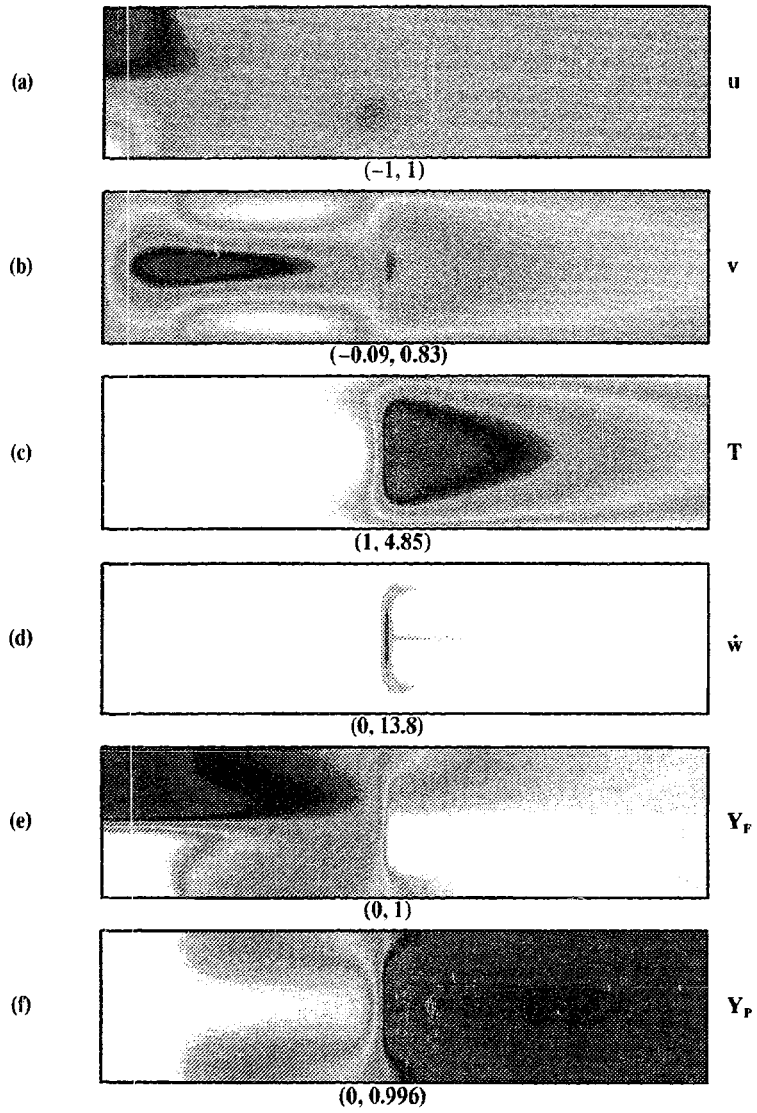

Fig. 7. Case II isocontours of (a) axial velocity; (b) radial velocity; (c) temperature; (d) reaction rate; (e) fuel mass fraction; and (f) product mass fraction. The minimum and maximum values of all variables are noted under each plot. Because this figure was generated by transformation of color plots to grey scale, the darkest tone does not correspond to the highest value.

respectively. The axisymmetric simulations reveal two-dimensional effects in the far field (the flow enters the domain in the axial direction but turns radially in the far field, as can be seen in figs. 6a and 6b), and a region of quasi one-dimensionality only up to a radial extent of about one tube radius along the stagnation plane.

As observed from the isocontours of temperature (Fig. 6c), reaction rate (Fig. 6d), fuel mass fraction (Fig. 6e), and product mass fraction (Fig. 6f), the case I steady state solution consists of a planar diffusion flame located at the stagnation plane, which, for this stoichiometric configuration, is exactly half way between the fuel and oxidizer exit plane ($z=0$). It can also be observed that product gases are being convected radially upstream because of a very weak recirculation, close to the top and bottom of the domain and between $0.5 < r < 1.25$, shown by the white regions in Fig. 6b.

The induction time for case II is longer than that of case I, and the reactant gases do not react immediately as they meet at the stagnation plane; instead, they flow radially outwards without reacting, and at the same time mix by diffusion and convection (as can be observed in Fig. 7b, there exists a small recirculation region in both the upper and the lower part of the domain, between $0.5 < r < 1.75$). Figures 7e and 7f show fuel and product mass fraction isocontours, respectively, (the fuel and oxidizer mass fraction isocontours being exactly antisymmetric with respect to the stagnation plane), and indicate that fuel diffuses into the oxidizer side and vice versa. Subsequently, at a radial location $r \approx 1.86$, the reactants form a triple flame structure, consisting of a premixed flame sitting normal to the flow direction and a diffusion flame trailing the premixed one (Fig. 7d). The top part of the premixed flame is fuel rich, whereas the lower one is fuel lean and the flame is curved towards the product gases because its maximum strength is at $z=0$ (where the concentration of the reactant gases is closer to stoichiometric). The trailing diffusion flame is much weaker than the leading premixed flame, starting exactly at the point where the fuel rich and fuel lean parts meet. In addition, as can be observed from the temperature and product mass fraction isocontours (Figs. 7c and 7f, respectively), both enthalpy and product gases are convected radially upstream because of the weak recirculation.

To illustrate more clearly the difference between the two flame configurations corresponding to cases I and II, temperature, species concentrations and reaction rates are plotted across the flame, which is along the axis of symmetry $r=0$ for case I (planar diffusion flame), and along the stagnation plane $z=0$ for case II (annular premixed flame), in Figs. 8 and 9, respectively. The flame profile for case I has the typical structure of a one-dimensional diffusion flame, whereas that of case II shows the reactant

gases approaching the flame zone in stoichiometric proportions along the stagnation line, and therefore forming a premixed flame. The maximum normalized value of temperature inside the flame zone is 4.094 for case I, and 4.85 for case II, whereas the reaction rate maxima are 17.15 and 13.8 respectively. Since the temperature of the cold gases is $T=1$ and the non-dimensionalized heat of the reaction is $h^0=4$, the adiabatic flame temperature for both problems is 5. Consistent with classical asymptotic results in combustion literature [Williams (1985)] which predict thinner reaction zones and higher flame temperatures for higher activation energies, the maximum temperature for case II is higher than the one for case I inside the flame. In addition, at the steady state, the total integral of the reaction rate over the domain, $\int_\Omega \rho\dot{w}'\,dv$, is limited for both cases I and II by the total fuel (or oxidizer) mass flux $\pi D^2\dot{m}_F/4$, where $\dot{m}_F=\rho U=0.5$ is the mass flux per unit area. This maximum value can only be achieved if the fuel and oxidizer are completely consumed during the reaction; the amount of reactants that exit the domain unburned is approximately 3.5% for both cases I and II.

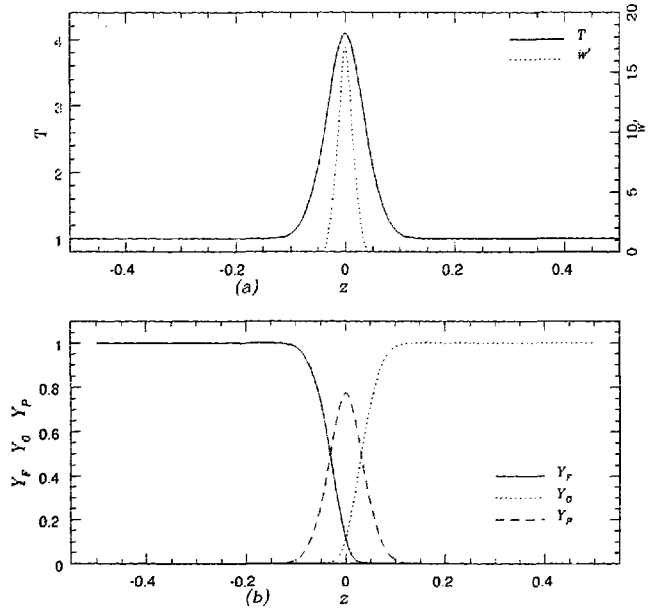

Fig. 8. (a) Variation of temperature and reaction rate; (b) species mass fractions along the line $r=0$ for case I.

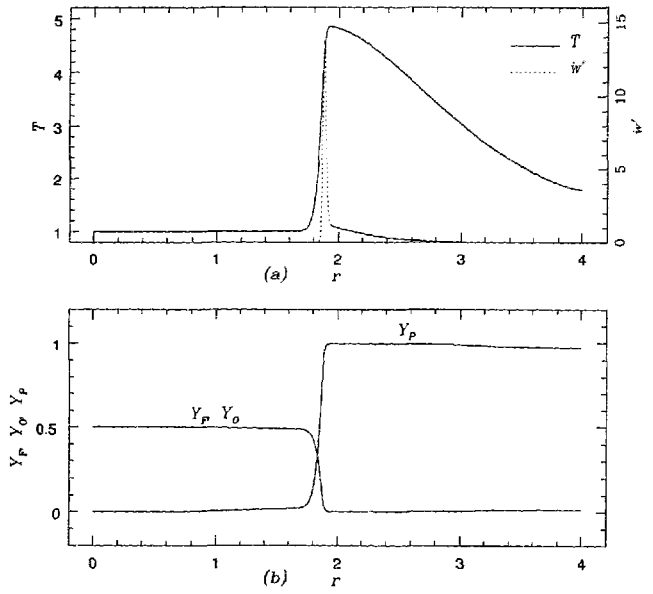

Fig. 9. (a) Variation of temperature and reaction rate; (b) species mass fractions along the line $z = 0$ for case II.

In case II, since the mean velocity of the reactant gases decreases radially (because of the increasing area) as roughly $1/r$, the premixed flame can stabilize itself at the location where the flame speed matches the local flow velocity. An estimate of this can be obtained as follows: the "burning rate eigenvalue" can be obtained as $(\rho S_L) = \rho_b(\dot{w}'_{\max}\alpha(T_b))^{1/2}$, where $\dot{w}'_{\max}$ is the maximum value of the reaction rate $\dot{w}'$, and ρ_b and $\alpha(T_b)$ are the values of density and heat diffusivity evaluated at the maximum temperature T_b. Here, the maximum flame temperature is $T_b = 4.85$, the maximum reaction rate is 13.8 (at approximately $r = 1.89$), $\alpha(T_b) = 0.024$, and $\rho_b = 0.206$, resulting in $(\rho S_L) \approx 0.12$. On the other hand, an estimate of the local mass flow rate (ρv) for strained flames can be obtained by using the density and velocity normal to the flame (in this case radially) evaluated at the inflection point of the temperature profile. Here, the inflection point of the temperature profile is located at about $r = 1.82$ where the values of the density and radial velocity are 0.53 and 0.23, respectively; therefore the value of (ρv) is very close to 0.12 as well.

Trailing the premixed annular flame, there exists a weak diffusion flame along the stagnation plane; this weaker reaction zone is also evident

in Fig. 9a, as a long tail in the reaction rate profile after the premixed peak at about $r = 1.89$. Profiles of reaction rate and species mass fractions across this reaction zone are shown in Fig. 10: fuel and oxidizer diffuse from the fuel rich and fuel lean side, respectively, into the weak reaction zone. The reaction rate peaks on both sides of the diffusion flame correspond to the top and bottom curved parts of the annular premixed flame (see Fig. 7d). As can be observed, the diffusion reaction zone is at least an order of magnitude weaker than the main premixed reaction zone [the maximum reaction rate being $\mathcal{O}(1)$ instead of $\mathcal{O}(10)$].

These two axisymmetric simulations reveal two-dimensional effects in the far field and also demonstrate that, even for simple transport and a one-step reaction mechanism, a mere change of the Damköhler number and the overall activation energy, can change the structure of a non-premixed flame from a nearly one-dimensional planar diffusion flame into an annular triple flame.

Such a transition has been observed experimentally [Papas (1995)]. However, this kind of behavior can only be observed for high activation energy fuels (i.e., methane) without inert co-flows around the fuel and

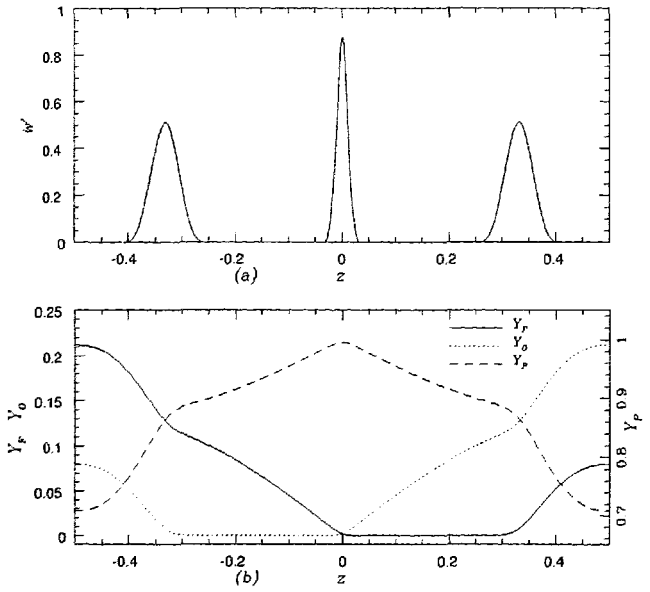

Fig. 10. (a) Variation of reaction rate; (b) species mass fractions along the line $r = 2.05$ for case II.

oxidizer streams, which are usually introduced in experiments to confine reaction in the local region between the reactant exists. The parameters used for case II can be thought of as corresponding to a reactant temperature of $500K$ and activation temperature of $20,000K$, which are comparable to the oxidation of methane.

This new capability of analyzing the opposed-jet flame offers a new means to validate previous one-dimensional numerical simulations. Since our new model is capable of handling detailed transport, variable fluid properties, and realistic chemical kinetics, it also offers an attractive new way to analyze data obtained in these experiments, and to assist in the design and optimization of these experiments.

Note that, although here we only report the results of non-premixed flames generated by the opposed-jet configuration, our numerical model can also be used to analyze strained premixed flames generated by the same experimental configuration. These flames are also of importance, as almost all modern data on freely propagating one-dimensional premixed flames are obtained from such experiments, which are also analyzed only by one-dimensional models (see for example the Sandia flame code Kee *et al.* (1985), or Law (1988)).

4.3. Porous Sphere

A droplet or particle burning in an oxidizer stream, which is another important configuration in combustion, can be analyzed by our numerical model. Here, we report the results of two model problems which physically correspond to a porous sphere burner, issuing fuel into an oxidizer stream, which is sufficiently hot to ignite the reactants, forming flames with different structure. The spectral element meshes used for these calculations (showing elements only) are shown in Fig. 11, and consist of 220 elements with 5×5 collocation points within each element (Fig. 11a), and 250 elements with 7×7 collocation points (Fig. 11b). The second mesh was designed after the location of the flame zone was identified using the first mesh, and was then refined to adequately resolve all scales.

The temperature of the hot oxidizer stream equals 2 and enters the domain from the left side with a velocity of 1. The cold fuel issues from the porous sphere with a radial velocity equal to 10% of the free stream velocity, at a temperature equal to 1. The simulations proceeded in the same way as for the opposed jet: the cold flow was first advanced to a steady state, and then the reaction rate term was turned on. For this case, there was no need for a high temperature strip as an initial condition, since the oxidize enters the domain with a temperature high enough to start the reaction.

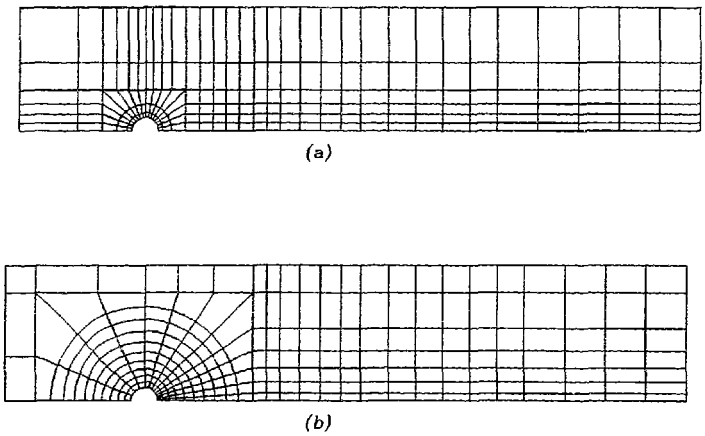

Fig. 11. Spectral element grids used for the simulation of the reactive flow around a porous sphere: (a) mesh with 220 elements (5×5 collocation points per element), and $-4.5 < z < 25$, $0 < r < 4.5$. (b) mesh with 250 elements (7×7 points per element), and $-5 < z < 20$, $0 < r < 5$.

The two model simulations reported here, differ only in the value of the overall activation temperature which was 12.5 in case I and 15 in case II. The other parameters, the Reynolds number (based on the free stream velocity, diameter of the sphere, and the kinematic viscosity of the oxidizer at $T = 2$) and pre-exponential Damköhler number were equal to 50 and 1,000, respectively.

In case I, the overall activation energy is sufficiently low that after the initial transient processes, a steady envelope flame establishes itself around the particle, as shown in Figs. 12a and 12b in terms of temperature and reaction rate isocontours. The maximum temperature inside the flame zone is equal to 4.24, whereas the maximum value of the reaction rate is equal to 2.51. The adiabatic flame temperature is equal to 5.5 (the temperature of the reactant gases is 1 and 2 respectively, whereas the non-dimensionalized heat of reaction is equal to 4). The one-step reaction, and corresponding reaction rate expression are the same as expressions (4.24) and (4.25) of the previous section, respectively, and the physical properties of all species are assumed to be equal.

In the second case, with increased activation energy and correspondingly longer chemical induction time, instead of an envelope closed flame, we see the establishment of a wake type flame (similar in nature to a premixed flame) as shown in Figs. 13a and 13b. The maximum values of temperature inside the flame zone and reaction rate for this case are equal to 4.72 and 2.90, respectively. Because the fuel exiting from the porous

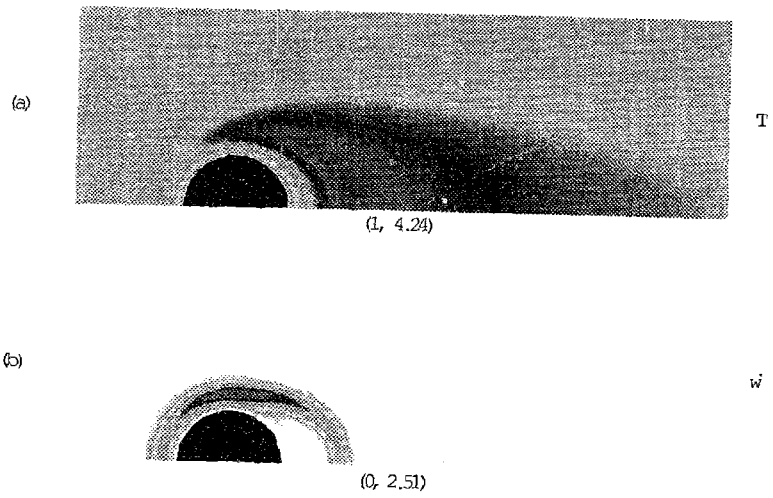

Fig. 12. (a) Isocontours of temperature; (b) reaction rate for the porous sphere case I with $T_1 = 12.5$. Because this figure was generated by transformation of color plots to grey scale, the darkest tone does not correspond to the highest value.

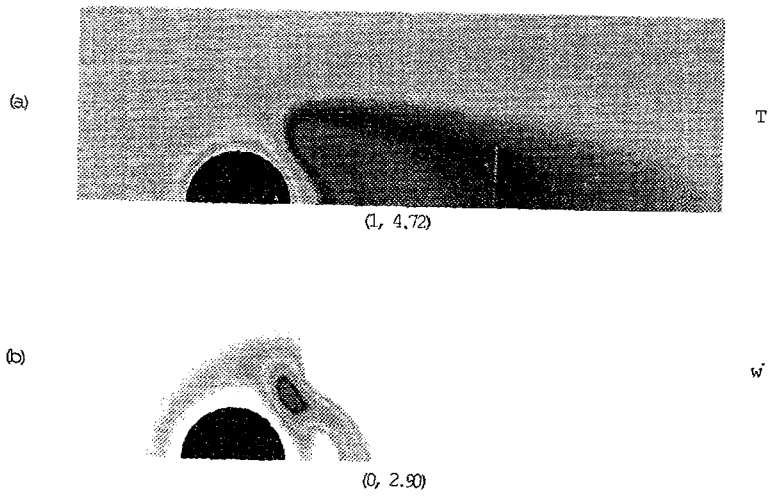

Fig. 13. (a) Isocontours of temperature; (b) reaction rate for the porous sphere case II with $T_1 = 15$. Because this figure was generated by transformation of color plots to grey scale, the darkest tone does not correspond to the highest value.

sphere is completely consumed in both cases due to the reaction, the total integral of the reaction rate, $\int_\Omega \rho\dot{w}'\,dv$ over the whole domain is the same in both cases at the steady state and equals $2\pi\dot{m}_F$, where $\dot{m}_F = 0.1$ is the mass flux of the fuel per unit area being issued from the surface of the sphere. This quantity reflects the total burning rate of the system. As in the opposed-jet configuration, although the total burning rate here is the same in both cases, the maximum temperature is higher for case II than for case I.

Similar calculations using realistic transport properties and elemental chemical kinetics have also been performed, and reported elsewhere [Lee *et al.* (1996b, 1997); and Lee (1996)].

5. CONCLUSIONS

A new method for the simulation of low Mach number combustion, which combines both accuracy and numerical efficiency, and which should be applicable to a wide range of combustion problems in the future, is presented. The numerical accuracy of the method has been analyzed asymptotically for splitting errors; the analysis of a more sophisticated model problem can be found elsewhere [Tomboulides and Orszag (1997)]. We have illustrated the application of this method to problems involving flames in opposed jet configurations and porous sphere burners. Applications of the method to problems involving detailed transport and comprehensive chemistry have also been performed and are reported in [Lee *et al.* (1996a); and Lee (1996).]

ACKNOWLEDGMENTS

This work was supported by DARPA/ONR under URI grant N00014-92-J-1796 and by NASA-Lewis under the Cooperative Agreement NCC3-487. We would like to thank Dr. R. A. Yetter and Professor F. L. Dryer for helpful discussions and comments. Most of the computations were performed on local resources at Princeton University and at the Cray J90 of the Swiss Federal Institute of Technology.

REFERENCES

Behrendt, F., Goyal, G., Maas, U., and Warnatz, J. (1992). Numerical study of two-dimensional effects associated with laser-induced ignition in hydrogen-oxygen mixtures, *24th Int. Symp. Combust.*, The Combustion Institute, p. 83.

Bender, C. M., and Orszag, S. A. (1978). *Advanced Mathematical Methods for Scientists and Engineers*, McGraw-Hill Publ. Co.

Canuto, C., Hussaini, M., Quarteroni, A., and Zang, T. (1987). *Spectral methods in Fluid Dynamics*, Springer-Verlag.

Cho, S., Yetter, R., and Dryer, F. (1992). A computer model for one-dimensional mass and energy transport in and around chemically reacting particles, including complex gas-phase chemistry, multicomponent molecular diffusion, surface evaporation and heterogeneous reactions. *J. Comput. Phys.* **102**, 160.

Chu, B. T., and Kovasznay, L. S. G. (1958). Non-linear interactions in a viscous heat-conducting compressible gas. *J. Fluid Mech.* **3**, 494–514.

Dwyer, H. (1990). Calculation of low mach number reacting flows. *AIAA* **28**, 99.

Dwyer, H., and Sanders, B. (1988). Calculations of unsteady reacting droplet flows. *22th Int. Symp. Combust.*, The Combustion Institute, p. 1923.

Ern, A., Douglas, C., and Smooke, M. (1994). Parallel computation of laminar diffusion flames. The Eastern States Section of the Combustion Institute, Dec 5-7, Clearwater Beach, Florida.

Gear, W. C. (1971). *Numerical Initial Value Problems in ordinary Differential Equations*, Prentice-Hall Publ. Co.

Gottlieb, D., and Orszag, S. A. (1977). *Numerical Analysis of Spectral Methods: Theory and Applications*, SIAM, Philadelphia, Pennsylvania.

Hindmarsh, A. C. (1983). ODEPACK, A systematized collections of ODE solvers. *Scientific Computing*, IMACS/North-Holland Publ., pp. 55–64.

Karniadakis, G. E., Bullister, E. T., and Patera, A. T. (1985). A spectral element method for solution of two-and three-dimensional time dependent Navier-Stokes equations. *Finite Element Methods for Nonlinear Problems*, Springer-Verlag, p. 803.

Karniadakis, G. E., Israeli, M., and Orszag, S. A. (1991). High-order splitting methods for the incompressible Navier-Stokes equations. *J. Comput. Phys.* **97**, 414.

Kee, R. J., Grcar, M. D., and Miller, J. A. (1985). A fortran program for modeling steady laminar one-dimensional premixed flames, Sandia National Laboratory Report SAND85-8240.

Law, C. K. (1988). *22th Int. Symp. Combust.*, The Combustion Institute, pp. 1381–1402.

Lee, J. (1996). Simulations of two-dimensional chemically reactive flows. Ph.D. thesis, Princeton University.

Lee, J., Yetter, R., and Dryer, F. (1995). Transient numerical modeling of carbon particle ignition and oxidation. *Combust. Flame* **101**, 387.

Lee, J., Yetter, R., and Dryer, F. (1996a). Numerical simulation of laser ignition of an isolated carbon particle in a quiescent environment, *Combust. Flame* **105**, 591.

Lee, J., Tomboulides, A. G., Orszag, S. A., Yetter, R., and Dryer, F. (1996b). A transient two-dimensional chemically reactive flow model: Fuel particle combustion in a nonquiescent environment. *26th Int. Symp. Combust.*, The Combustion Institute.

Lee, J., Tomboulides, A. G., Orszag, S. A., Yetter, R., and Dryer, F. (1997). Integrated asymptotic analysis and numerical simulation of laminar flow reactors. *Combust. Sci. Tech.*, submitted.

Lutz, A. E., Kee, R. J., and Grcar, J. F. (1994). Program for computing oppose-flow diffusion flames, Sandia National Laboratory Report.

Maday, Y., and Patera, A. T. (1987). Spectral element methods for the Navier-Stokes equations. *ASME. State-of-the-Art Surveys in Computational Mechanics.*

Megaridis, C., and Sirignano, W. (1992). Multicomponent droplet vaporization in a laminar convective environment. *Combust. Sci. Tech.* **87**, 27.

Oran, E. S., and Boris, J. P. (1987). *Numerical Simulation of Reactive Flow*, Elsevier Science Publ. Co.

Orszag, S. A., Israeli, M., and Deville, M. O. (1986). Boundary conditions for incompressible flows. *J. Sci. Comp.* **1**, 75.

Papas, P. (1995). Personal communication.
Patera, A. T. (1984). A spectral element method for fluid dynamics: Laminar flow in a channel expansion, *J. Comput. Phys.* **54**, 468.
Patnaik, G., Kailasanath, K., Oran, E., and Laskey, K. (1988). Detailed numerical simulations of cellular flames. *22nd Int. Symp. Combust.*, The Combustion Institute, p. 1517.
Patnaik, G., Sirignano, W., Dwyer, H., and Sander, B. (1985). A numerical technique for the solution of a vaporizing fuel droplet, *10th Int. Colloquium on the Dynamics of Explosions and Reactive Systems*, Berkeley, California.
Poinsot, T., Candel, S., and Trouve, A. (1996). Applications of direct numerical simulation to premixed turbulent combustion, *Prog. Energy Combust. Sci.* Pergamon Press, **21**, 531–576.
Rehm, G. R., and Baum, H. R. (1978). The equations of motion for thermally driven flows, *J. Res. National Bureau of Standards* **83** (3), 297–308.
Ronquist, E. M. (1988). Optimal spectral element methods for the unsteady three-dimensional incompressible Navier-Stokes equations, Ph.D. Thesis, Massachusetts Institute of Technology.
Sivashinsky, G. J. (1979). Hydrodynamics theory of flame propagation in an enclosed volume. *Acta Astronautica* **6**, 631–645.
Smooke, M., Mitchell, R., and Keyes, D. (1989). Numerical solution of two-dimensional axisymmetric laminar diffusion flames, *Combust. Sci. Tech.* **67**, 85.
Tomboulides, A. G., Israeli, M., and Karniadakis, G. E. (1989). Efficient removal of boundary-divergence errors in time-splitting methods, *J. Sci. Comp.* **4**, 291.
Tomboulides, A. G., and Orszag, S. A. (1997). A quasi two-dimensional benchmark problem for low mach number compressible codes. (in press).
Williams, F. A. (1985). *Combustion Theory*, Benjamin/Cummings Publ. Co. Second Edition.
Xu, Y., Smooke, M., and Long, M. (1993). Primitive variable modeling of multidimensional laminar flames, *Combust. Sci. Tech.* **90**, 289.